Electron-beam ion-trap spectra of tungsten in the EUV

S.B. Utter, P. Beiersdorfer, and E. Träbert

Abstract: At the Livermore electron-beam ion-trap facility, extreme-ultraviolet spectra of tungsten have been recorded in the wavelength range 40–85 Å. The electron-beam energy was varied systematically to identify the individual spectra of Rb-like W^{37+} to Cu-like W^{45+}. About 60 spectral features have been identified.

PACS Nos.: 32.30Rj, 39.30+w, 31.50+w

Résumé : On a varié systematiquement l'energie du faisceaux des electrons dans un piège ionique à faisceaux electronique pour la production des spectra rayon X (40 à 85 Å) des ions isoélectroniques de Rb (W^{37+}) à Cu (W^{45+}). Guidé par des calculs relativistiques de la structure atomique, on a identifié près de 60 des transitions.

1. Introduction

Tungsten (W) is of great interest for its intricate relationship to fusion plasmas, since many components of present-day and planned future generation tokamaks are made of tungsten because of its advantageous physical properties. As tokamak systems become increasingly more sophisticated, the ability to predict and monitor plasma properties becomes imperative. It is important, then, to have accurate data on which to base these predictions. Since tungsten is usually present as an impurity in the plasma, a significant fraction of the energy may be exhausted via the radiation emitted by tungsten ions [1, 2]. The intermediate charge states of tungsten from Rb-like W^{37+} to Cu-like W^{45+} are some of the most prominent in plasmas with ion temperatures of a few keV. These ions radiate a significant portion of their spectra in the extreme ultraviolet (EUV) from 40 to 85 Å. The same spectral region has been covered in investigations of laser-produced plasmas [3, 4].

In hot plasmas there usually are ions from various elements and in so many charge states that it is often not feasible to identify individual spectra. An electron-beam ion trap [5], in contrast, cannot only produce spectra that are dominated by a single element, but it can, by step-wise variation of the electron-beam energy, provide data for the definite association of each line to the ionization energy of its source ion and, therefore, the charge state. Precise measurements of this type have been made on tungsten, on the above charge states and covering the aforementioned wavelength range. Stepping the energy of the electron beam in the Livermore EBIT-II device from 1.7 to 3.0 keV has resulted in charge-state identifications of more than 60 lines (this work), classifying most of these with the aid of

S.B. Utter,[1] P. Beiersdorfer, and E. Träbert.[2] Division of Physics and Advanced Technologies, Lawrence Livermore National Laboratory, Livermore, CA 94550-9234, U.S.A.

[1] Present address: Spectra-Physics, Mountain View, CA 94039, U.S.A.
[2] Corresponding author (e-mail: traebert@ep3.ruhr-uni-bochum.de).

published calculational results [6].

This study complements two studies of the EUV spectrum of tungsten performed in parallel to our work at the Berlin EBIT (one study of the adjacent range of lower charge states, on W^{25+} to W^{36+}, the other one of the W ions in charge states from $q = 21+$ to $q = 45+$) [7, 8], and our own study of a prominent line in the visible spectrum of the Ti-like ion W^{52+} [9]. Comparable data have been obtained on the electron-beam ion trap EBIT-II for the EUV spectrum of gold [10]. Although there is an overlap of the present report with the ion-charge-state coverage of the Berlin work, the experimental conditions of ion preparation and of the detection systems are different, so that an independent data set emerges. A comparison of the results then provides a realistic estimate of the spectroscopic capabilities of electron-beam ion traps in the EUV.

2. Theoretical predictions

While many measurements of particular lines and theoretical predictions of transitions from inter-mediate charge-state ions have been reported in the last 20 years, the most complete compilation of the wavelengths and intensities of these lines in tungsten appears to be that by Fournier [6], where transition wavelengths were derived from ab initio atomic-structure calculations. These calculations were performed with the graphical angular-momentum coupling code ANGLAR and the fully relativistic parametric-potential code RELAC. Of particular interest to this work are the predictions, therein, of the wavelengths and intensities of the lines from Rb-like W^{37+} to Cu-like W^{45+} ions in the spectral range from 40 to 85 Å. Fournier's predictions for ions of these charge states are displayed in Fig. 1. We have convolved the lines in this figure with a Gaussian function with a FWHM the same as the lines measured with our flat-field spectrometer (FFS) described below. The peak of the Gaussian is proportional to the calculated line intensity for each transition computed in a collisional-radiative model for a plasma with an electron temperature 60% of the ionization potential for each ion. All of the spectra are displayed on a common intensity scale, with the exception of the spectra of the Zn- and Ge-like ions which are more suppressed than the others.

Most of the strong spectral lines correspond to $\Delta J = 1$ transitions and can be sorted into two groups, those near 45 Å and those near 60 Å. The group near 45 Å is composed of 4p–4d transitions. In the 60 Å region, 4s–4p and 4p–4p transitions dominate. Several transitions of similar type can be traced along the changing charge states as the electron core changes. For instance, the core of the Cu-like charge state is a closed $n = 3$ shell, and the transition $(4p-)^1{}_{J=\frac{1}{2}} - (4d-)^1{}_{J=\frac{3}{2}}$ (the notation is explained in Sect. 3) has a predicted wavelength of 49.165 Å — note that this is not a transition to the ground state. Adding another electron to the core produces the Zn-like charge state, and a similar transition $(4p-)^1{}_{J=1} - (4d-)^1{}_{J=2}$ is predicted to occur at a slightly shorter wavelength (higher energy), $\lambda = 48.412$ Å. The trend continues with the corresponding transitions in the Ga-like spectrum at 47.637 Å and in the Ge-like spectrum at 46.805 Å, where the corresponding transition has now become one to the ground state of the ion. As-, Se-, Br-, and Kr-like spectra follow suit with similar transitions predicted at 46.794, 46.294, 46.188, and 46.142 Å, respectively. Identification of this line within a particular ion's spectrum, the strongest in many of these charge states, facilitates the identification of the corresponding transition in neighboring charge-state ions, since the wavelengths sequentially decrease.

The intensity of such lines is also a key to the identification. In a low-density, collisionally excited plasma, transitions to the ground state will tend to be more intense than transitions to other excited states. This is exemplified by the transition just mentioned, and can be seen in Fig. 1. For the Cu- and Zn-like charge states (where it is not a ground-state transition), the transition is predicted to be rather weak, while it should be one of the strongest in the remaining ions of the list. The relative intensities of the measured lines depend on many additional factors, including the response function of the CCD camera and the charge balance of the various ions present. Nonetheless, the line-intensity predictions need to be corroborated at least qualitatively, if they are to be useful in future calculations of plasma

Fig. 1. Simulated spectra based on the predictions by Fournier [6] for N-shell ($n = 4$) transitions in nine ion-charge states of tungsten. Each of the predicted lines was convolved with a Gaussian function of 0.12 Å width (FWHM).
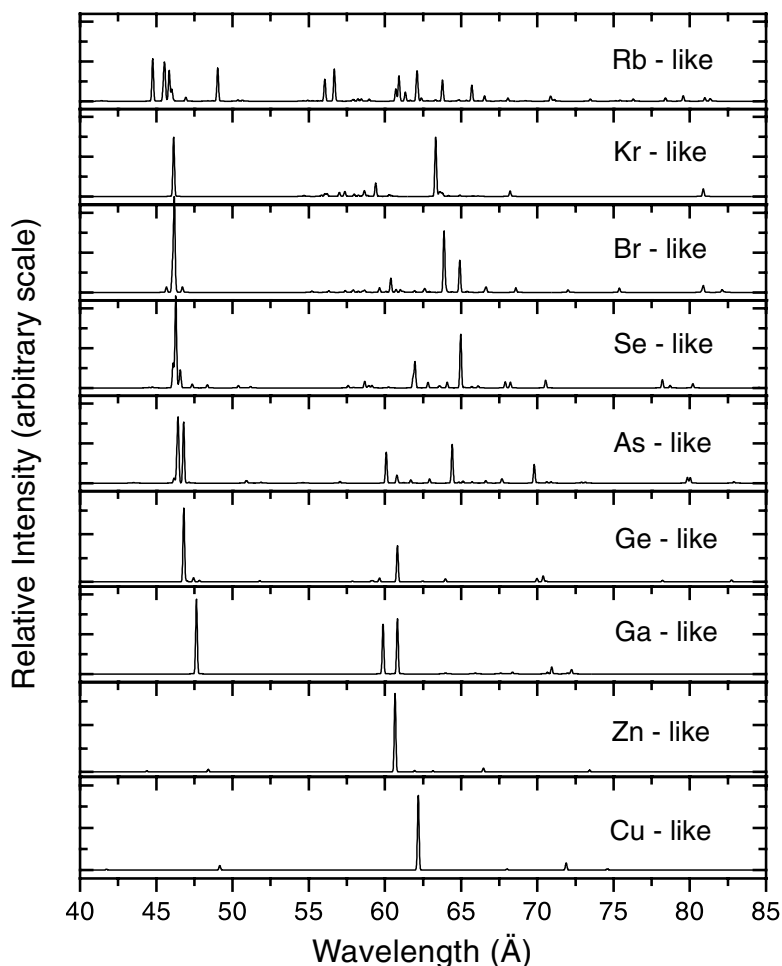
parameters and radiative power loss.

3. Experiment

The measurements were done at the EBIT facility at the University of California Lawrence Livermore National Laboratory. Of the two electron-beam ion traps available, EBIT-II, the lower electron-beam energy device, was used in this experiment. Electron-beam energies of about 3 keV were sufficient to produce ions in all the charge states of present interest.

Tungsten ions produced in a metal vapor vacuum arc (MeVVA) ion source were injected into EBIT-II and then held in the trap by the combination of electric fields of the drift tubes, the attraction and space-charge compensation of the electron beam, and the 3 T magnetic guide field. The impinging fast electrons then continue to ionize the trapped ions (in competition with some electron capture by recombination or charge exchange). The highest charge state reached is the lowest one whose ionization potential exceeds the electron-beam energy. The electron-beam energy, therefore, can be varied so as to change the charge-state distribution. In particular, it can be lowered below the production threshold of a given ion. Sequences of such experiments at different electron-beam energies thus yield spectra that differ by the contribution of a single-charge-state ion.

The spectral measurements employed a flat-field spectrometer (FFS) [11] equipped with a variable-line spaced grating [12] of about 2400 ℓ/mm. This grating had been tested to show practically only first-diffraction order lines. The grating disperses a spectrum onto a cryogenically cooled CCD camera equipped with a 25 mm square CCD chip with 1024×1024 pixels of 24 μm size and with 1 μm gaps in between. This size was sufficient to simultaneously record the full spectral range of interest. The spectrometer images the volume of the electron beam (with a beam diameter of about 60 μm [13]), without an entrance slit, onto the detector, where the image is about 2 pixels wide.

CCD camera chips are sensitive to cosmic rays, leading to comparatively high amounts of charge stored in just a few pixels. These pixels exceed the signal level in the regular data pixels by several orders of magnitude and are easily recognized. However, real data might be hidden underneath, which is why exposure times have to be short enough to prevent the accumulation of too many cosmic-ray events in a single spectrum. Filtering by automatic routines (checking for gross deviations from the average signal level in one or a few pixels within a group of pixels) and by individual human inspection was employed to remove these spurious events before further evaluation. Balancing the wish for long integration times to obtain a clear signal above the read-out noise of the CCD and the need to correct for cosmic events, the typical exposure time chosen was 20 min per spectrum. Multiple exposures were taken under the same conditions until enough statistics were accumulated to facilitate line fitting. The recording of multiple spectra of the same spectral region also serves to assure a spectral coverage that is unimpeded by the vagaries of the filtering process of the individual spectra. Because of the nonlinearities of the detector response near the edge, only a central zone of about 950 pixels width was evaluated. Spectra along parallel, about 250 pixels wide strips, were binned across the direction of dispersion. By evaluating these strip spectra individually, sharper line images could be retrieved than from full binning, because some of the lines were slightly curved and slanted, even after extensive focusing efforts.

In an electron-beam ion trap, heavy, highly charged ions are trapped most easily. Tungsten ions will thus displace most light element contaminants, which are notable even at the typical EBIT-II vacuum pressure of better than 10^{-10} Torr (1 Torr = 133.3 Pa). Of these, lines of H- and He-like ions of carbon, oxygen, and nitrogen were used for wavelength calibration in the range $20 - 40$ Å. At times, a gas injector fed neon into EBIT-II to provide calibration lines (mostly from Li-like ions) also in the long-wavelength part of the spectrum.

EBIT-II was run in a steady-state mode throughout these measurements. That is, the electron-beam current I_{beam} and energy E_{beam} were kept constant throughout the total data integration time. I_{beam} was kept at a value of 60 mA during tungsten and background data acquisition. Although at the higher electron-beam energies the electron-beam current could have been increased significantly, this would have made comparison of the line intensities in successive steps less clear, since the line intensities and the space-charge effects are also a function of I_{beam}. Ideally, it is the emissivity ϵ, that is, the photon emission rate, that should remain the same during the measurements. This can be written as

$$\epsilon = f_{ie} n_e n_i \sigma_i v_e$$

where f_{ie} is the electron–ion overlap, n_e is the electron density, n_i is the ion density, σ_i is the ion cross section, and v_e is the speed of the electrons in the beam. Since the beam current can be written as

$$I_{beam} = n_e v_e A$$

where A is the cross-sectional area of the electron beam, ϵ can be rewritten in the form

$$\epsilon = \frac{f_{ie} n_i \sigma_i I_{beam}}{A}$$

Even assuming that $f_{ie} n_i / A = $ constant, which is true as a first-order approximation for the small energy variation considered here, it is known that σ_i varies as a function of energy. From the lowest to

the highest beam energies in these measurements, this value may have changed by as much as 25%, which directly affected the total number of electron–ion collisions. For measurements at neighboring energies that differ only by 50 – 100 V the change in σ_i is small. Settings of $I_{beam} = 27$ mA and $E_{beam} = 1.04$ keV (appropriate for creating the Li-like species) were used during the acquisition of neon calibration spectra.

The electron-beam energies result from the sum U_{appl} of the overall acceleration voltage when forming an electron beam and the potential of the middle drift tube of EBIT. However, there is a correction to this sum that depends on the space charge of the electron beam itself. This space charge, a function of I_{beam}, U_{appl}, and r, the radial distance from the center of the beam, can only reduce the net potential. Details have been explained, for example, by Widmann [14]. A "rule-of-thumb" approximation of the space-charge potential V_{SC} at the center of the beam is $V_{SC} = 2.5\ I_{beam}/\sqrt{U_{appl}}$, with I_{beam} in mA, U_{appl} in kV, and the result in volts. The space-charge potential at the edge of the beam is thus reduced by about 75 V in our case. The effect results in a slight smearing out of the electron-beam energy and a slight shift of the apparent ionization thresholds. The electron-beam energy range from 1.7 to 3.0 keV was covered in 23 steps of either 50 or 100 V. All of the beam energies listed in this work are defined as $E = e * (U_{appl} - U_{SC})$, where e is the elementary charge unit.

To distinguish background lines from W lines, and to obtain a measure of the background integrated by the CCD detector, a sequence of exposures including background, calibration, and W data acquisition was implemented which for each cycle required about 3 h of acquisition time. The cycle of calibration $\rightarrow$ W $\rightarrow$ background $\rightarrow$ W $\rightarrow$, etc. was repeated until the entire energy range was covered.

To obtain a measure of the stray light reaching the detector (mainly coming from the hot electron gun), trapping was prevented by raising the potential of the middle drift tube to a value higher than that of the top drift tube ("inverting the trap" [9, 15]). The background spectra with no trapping were smoothed (represented by an approximate curve) and then subtracted from the spectra with trapping, thus establishing a baseline from which the spectral lines could be measured.

3.1. Wavelength calibration

Our EBIT-II allows for rapid switching from injecting metals from the MeVVA to gas injection. This permits the regular introduction of light gases to be used for in situ calibration. Ideally, all calibration would be performed using wavelengths (energies) from transitions that have been both precisely measured and numerically calculated. However, precision measurements of spectra throughout the EUV are not yet available. Theoretically predicted (and experimentally confirmed) wavelengths are extremely precise for transitions in H-like ions, and very good for those in He-like ions, but are worse for charge states beyond. In the wavelength region of these measurements, the spectrum up to about 45 Å is covered by several He-like transitions of O, N, and C. Transitions of He-like Li, Be, or B would extend the limit to longer wavelengths, but there are technical reasons why these elements are difficult to study in EBIT-II. Therefore, transitions of Li-like Ne ions were used to calibrate the range from 55–85 Å. Although measurements of these lines have uncertainties of about 5 mÅ, the lines suffice for calibration. The limited knowledge of the calibration line wavelengths does, however, limit the certainty of these measurements, particularly near the longer wavelength end of the spectra. Eight of these known transitions were measured and their line centers were determined by fitting the peaks with Gaussian functions. A third-order polynomial was fit to this series of data to obtain a dispersion equation for the entire span of the subtended spectral range. The quality of the calibration was tested by fitting weaker, yet well known, "test" lines from the calibration gases. The statistical deviation of the test points was determined to be within approximately 4 mÅ of their accepted values. The statistical deviation of the residuals of the fitted points was measured to be close to 3 mÅ.

3.2. Intensity calibration

The intensity of spectral lines yields information about the state of the plasma from which they are emitted. For instance, certain transitions may be affected by the density of the plasma. Under certain circumstances, line intensities can give information about the charge-state abundance of ions, collisional cross sections, or recombination rates. For the purposes here, a measure of the absolute intensity was not necessary; a measurement of the relative intensity of spectral lines from within a single-charge state was sufficient. For this, only the reflectivity of the grating and the efficiency of the detector as functions of energy were needed.

Several recent studies of the efficiency of spectrometer systems in the EUV using CCD detectors have been reported of which the measurement by Saemann and Eidmann [16] is most closely related to the present work. Those authors obtained an absolute sensitivity calibration of a flat-field spectrometer in the wavelength range 10–70 Å by means of a laser-generated plasma of a well-known X-ray conversion. They implemented a 2400 ℓ/mm flat-field grating and a back-thinned CCD detector rather similar to ours. An independent measurement of the efficiency of the CCD detector resulted in a quantum-efficiency measurement of the detector itself. By unfolding this efficiency from the results from the spectrometer system they were able to obtain a result independent of the CCD as well. Their data revealed a severe dip in the efficiency curve near 42.5 Å that, in their case, was attributed to a thin oil layer on the surface of the imaging mirrors used in their spectrometer. Though such mirrors do not exist in the present spectrometer, our CCD detector is known to suffer contamination by a thin layer of oil (the result of pump oil from a vacuum accident). Indeed, the line-rich spectra of Kr that have been recorded with the same equipment [17] reveal a dip of the efficiency at the absorption edge of carbon. Consequently, the efficiency curve measured by Saemann and Eidmann appears to be quite applicable and has been used to adjust the measured line intensities. The "dip" only affects very few of the measured lines.

4. Experimental results

All of the data files were independently filtered for cosmic rays. The smoothed baseline was then subtracted from each spectrum, and the files of the same energy were summed. Each of the summed spectra was then analyzed by fitting the peaks with Gaussian functions. All of the fitted lines in a spectrum were constrained to have the same FWHM, but this parameter was optimized for each spectrum. The line centers (in channels) were converted to wavelength units using a third-order polynomial dispersion equation. By following the evolution of the line intensity of any line through a series of energies, the charge state from which the line emanated could be identified. Comparison of wavelengths with the calculations by Fournier [6] and with data from previous measurements [1–4] permitted us to identify most of the transitions. Tables 1 through 9 summarize the line identifications by charge state. The levels (lower and upper) listed in these tables use the following naming scheme, as described by Fournier [6].

In the intermediate charge states of tungsten, LS coupling is no longer appropriate. RELAC's intermediate-coupling calculations are carried out on the jj-coupling basis set. The jj orbitals nlj are represented by $nl+$ or $nl-$, where the $+$ indicates $j = l + 1/2$ and the $-$ indicates $j = l - 1/2$ (for example, this means $3d_{3/2} = 3d-$ and $3d_{5/2} = 3d+$). In the tables, when both nlj orbitals in a shell are full, the shell is represented by $(nl)^k$, where k is the maximum occupancy of the shell (for example, $(3d-)^4(3d+)^6 = (3d)^{10}$). These closed shells and subshells are actually omitted from the tables except where such an omission might result in confusion.

The nine tables are organized in the same way. First we list the atomic levels involved in the transition; then, the total J values of the lower and upper levels. Next the predicted (from Fournier) and measured (present experiments) wavelengths are listed. In parentheses, following the measured wavelengths, is a measure of the statistical uncertainty of each wavelength. The best lines have statistical errors that are less than 2 mÅ. Larger error bars (up to a factor of 10) result for lines that are either weak, or are blended with neighboring lines from the same or a near-by charge state. An additional 4 mÅ has been added to the uncertainty of each line due to the poorer accuracy of the calibration beyond 45 Å. Finally, the

Table 1. List of predicted and measured transitions in the Rb-like ion W^{39+} (ground state: $(4s)^2(4p)^6(4d-)^1$ $J = 3/2$). Wavelength predictions quoted are those by Fournier [6].

Level				Wavelength		Intensity	
Lower	Upper	J_l	J_u	Predicted	Measured	Pred.	Meas.
$(4d-)^1$	$(4p-)^1(4p+)^4(4d-)^2$	3/2	3/2	44.766	45.7810(22)	1.00	1.00
$(4d-)^1$	$(4p-)^1(4p+)^4(4d-)^1(4d+)^1$	5/2	3/2	45.480	46.0640(55)b	0.39	0.25
$(4d-)^1$	$(4p-)^1(4p+)^4(4d-)^1(4d+)^1$	5/2	7/2	45.556	46.0640(55)b	0.75	
$(4d-)^1$	$(4p-)^1(4p+)^4(4d-)^2$	3/2	5/2	49.030	49.6407(54)	0.78	0.58
$(4d-)^1$	$(4p)^6(4f-)^1$	3/2	5/2	56.055	56.8797(41)	0.52	0.35
$(4d-)^1$	$(4p-)^1(4p+)^4(4d+)^2$	3/2	5/2	56.680	57.7547(14)	0.38	0.23
$(4d-)^1$	$(4p-)^1(4p+)^4(4d-)^1(4d+)^1$	3/2	1/2	60.717	—	0.21	—
$(4d-)^1$	$(4p)^6(4f+)^1$	5/2	7/2	60.922	61.9200(83)b	0.59	0.15
$(4d-)^1$	$(4p)^6(4f-)^1$	5/2	5/2	61.340	61.9200(83)b	0.22	
$(4d-)^1$	$(4p-)^2(4p+)^3(4d+)^2$	5/2	5/2	62.090	63.4319(119)b	0.46	0.13
$(4d-)^1$	$(4p-)^2(4p+)^3(4d+)^2$	5/2	3/2	62.138	63.4319(119)b	0.34	
$(4d-)^1$	$(4p-)^2(4p+)^3(4d-)^1(4d+)^1$	3/2	3/2	63.775	64.8250(200)	0.50	0.16
$(4d-)^1$	$(4p-)^2(4p+)^3(4d-)^1(4d+)^1$	3/2	5/2	65.703	66.29252(147)	0.38	0.12
$(4d-)^1$	$(4p-)^2(4p+)^3(4d-)^2$	3/2	1/2	81.299	81.4573(89)b	0.02	0.05
$(4d-)^1$	$(4p-)^2(4p+)^3(4d-)^2$	3/2	3/2	81.359	81.4573(89)b	0.05	

Note: The "b" following a measured wavelength indicates a line blend.

Table 2. List of predicted and measured transitions in the Kr-like ion W^{39+} (ground state: $(4s)^2(4p)^6$ $J = 0$). Wavelength predictions quoted are those by Fournier [6].

Level				Wavelength		Intensity	
Lower	Upper	J_l	J_u	Predicted	Measured	Pred.	Meas.
$(4p)^6$	$(4p-)^1(4p+)^4(4d-)^1$	0	1	46.142	46.6703(12)	1.00	1.00
Unknown	Unknown	—	—	—	49.36511(57)	—	0.11
Unknown	Unknown	—	—	—	50.2057(64)	—	0.09
Unknown	Unknown	—	—	—	57.7171(70)	—	0.18
Unknown	Unknown	—	—	—	62.3659(43)	—	0.14
$(4p)^6$	$(4p-)^1(4p+)^4(4d+)^1$	0	1	63.326	63.8834(41)	0.96	0.22
$(4p)^6$	$(4p-)^1(4p+)^4(4d-)^1$	0	1	80.886	80.6420(226)	0.13	0.06

Table 3. List of predicted and measured transitions in the Br-like ion W^{39+} (ground state: $(4s)^2(4p-)^2(4p+)^3$ $J = 3/2$). Wavelength predictions quoted are those by Fournier [6].

Level				Wavelength		Intensity	
Lower	Upper	J_l	J_u	Predicted	Measured	Pred.	Meas.
$(4p-)^2(4p+)^3$	$(4p-)^1(4p+)^3(4d+)^1$	3/2	5/2	45.669	45.9539(26)	0.09	0.00
$(4p-)^2(4p+)^3$	$(4p-)^1(4p+)^3(4d-)^1$	3/2	1/2	46.069	46.8267(09)b	0.44	3.61
$(4p-)^2(4p+)^3$	$(4p-)^1(4p+)^3(4d-)^1$	3/2	3/2	46.181	46.8267(09)b	1.00	
$(4p-)^2(4p+)^3$	$(4p-)^1(4p+)^3(4d-)^1$	3/2	5/2	46.188	46.8267(09)b	0.55	
$(4p-)^2(4p+)^3$	$(4p-)^1(4p+)^3(4d-)^1$	3/2	5/2	50.010	50.6605(99)	0.05	0.17
$(4p-)^2(4p+)^3$	$(4s+)^1(4p)^6$	3/2	1/2	60.387	61.0499(29)	0.24	0.33
$(4p-)^2(4p+)^3$	$(4p-)^2(4p+)^2(4d+)^1$	3/2	5/2	63.877	64.6606(155)	1.00	1.00
$(4p-)^2(4p+)^3$	$(4p-)^2(4p+)^2(4d+)^1$	3/2	3/2	64.901	65.6575(59)	0.53	0.42
$(4p-)^2(4p+)^3$	$(4p-)^2(4p+)^2(4d-)^1$	3/2	5/2	80.892	81.1531(03)	0.11	0.21

Note: The "b" following a measured wavelength indicates a line blend.

Table 4. List of predicted and measured transitions in the Se-like ions W^{40+} (ground state: $(4s)^2(4p-)^2(4p+)^2$ $J = 2$). Wavelength predictions quoted are those by Fournier [6].

Level				Wavelength		Intensity	
Lower	Upper	J_l	J_u	Predicted	Measured	Pred.	Meas.
$(4p-)^2(4p+)^2$	$(4p-)^1(4p+)^2(4d-)^1$	2	1	46.102	46.3776(27)	0.46	0.57
$(4p-)^2(4p+)^2$	$(4p-)^1(4p+)^2(4d-)^1$	2	2	46.260	46.9573(21)b	0.80	3.36
$(4p-)^2(4p+)^2$	$(4p-)^1(4p+)^2(4d-)^1$	2	3	46.294	46.9573(21)b	1.03	
$(4p-)^2(4p+)^2$	$(4p-)^1(4p+)^2(4d-)^1$	2	3	47.359	47.6044(42)	0.07	0.71
$(4p-)^2(4p+)^2$	$(4p-)^1(4p+)^2(4d-)^1$	2	2	48.349	48.7460(56)	0.06	0.26
$(4p-)^2(4p+)^2$	$(4s+)^1(4p-)^2(4p+)^3$	2	1	58.674	59.5257(66)	0.12	0.42
$(4p-)^2(4p+)^2$	$(4s+)^1(4p-)^2(4p+)^3$	0	1	61.850	62.1934(163)	0.17	0.30
$(4p-)^2(4p+)^2$	$(4s+)^1(4p-)^2(4p+)^3$	2	2	61.973	62.6885(38)	0.48	0.74
$(4p-)^2(4p+)^2$	$(4p-)^1(4p+)^2(4d-)^1$	2	3	64.972	65.8729(25)	1.00	1.00
$(4p-)^2(4p+)^2$	$(4p-)^1(4p+)^2(4d-)^1$	2	2	70.545	71.1180(34)	0.15	0.23
$(4p-)^2(4p+)^2$	$(4p-)^1(4p+)^2(4d-)^1$	2	3	78.202	78.9521(121)	0.16	0.32

Note: The "b" following a measured wavelength indicates a line blend.

Table 5. List of predicted and measured transitions in the As-like ion W^{41+} (ground state: $(4s)^2(4p-)^2(4p+)^1$ $J = 3/2$). Wavelength predictions quoted are those by Fournier [6].

Level				Wavelength		Intensity	
Lower	Upper	J_l	J_u	Predicted	Measured	Pred.	Meas.
$(4p-)^2(4p+)^1$	$(4p-)^1(4p+)^1(4d-)^1$	3/2	3/2	46.438	47.0480(58)	0.94	0.73
$(4p-)^2(4p+)^1$	$(4p-)^1(4p+)^1(4d-)^1$	3/2	5/2	46.794	47.2873(81)	1.00	1.00
$(4p-)^2(4p+)^1$	$(4p-)^1(4p+)^1(4d-)^1$	3/2	3/2	50.894	51.0906(108)	0.04	0.04
$(4p-)^2(4p+)^1$	$(4s+)^1(4p-)^2(4p+)^2$	3/2	3/2	60.087	60.7285(11)	0.51	0.23
$(4p-)^2(4p+)^1$	$(4s+)^1(4p-)^2(4p+)^2$	3/2	5/2	64.413	64.8883(47)	0.63	0.18
$(4p-)^2(4p+)^1$	$(4p-)^2(4d+)^1$	3/2	5/2	69.796	70.1496(39)	0.30	0.08
$(4p-)^2(4p+)^1$	$(4p-)^2(4d-)^1$	3/2	3/2	80.029	80.8888(166)	0.09	0.02

Table 6. List of predicted and measured transitions in the Ge-like ion W^{42+} (ground state: $(4s)^2(4p-)^2$ $J = 0$). Wavelength predictions quoted are those by Fournier [6].

Level				Wavelength		Intensity	
Lower	Upper	J_l	J_u	Predicted	Measured	Pred.	Meas.
$(4s)^2(4p-)^2$	$(4s)^2(4p-)^1(4d-)^1$	0	1	46.805	47.1905(28)	1.00	1.00
$(4s)^2(4p-)^2$	$(4s)^2(4p-)^2(4p+)^1$	0	1	60.820	61.3039(60)	0.49	0.55
$(4s+)^1(4p-)^2(4p+)^1$	$(4s+)^1(4p-)^2(4d+)^1$	1	2	70.381	70.4349(65)	0.01	0.04
$(4s)^2(4p-)^1(4p+)^1$	$(4s)^2(4p-)^1(4d-)^1$	2	2	82.739	83.2887(39)	0.00	0.02

Table 7. List of predicted and measured transitions in the Ga-like ion W^{43+} (ground state: $(4s)^2(4p-)^1$ $J = 1/2$). Wavelength predictions quoted are those by Fournier [6].

Level				Wavelength		Intensity	
Lower	Upper	J_l	J_u	Predicted	Measured	Pred.	Meas.
$(4p-)^1$	$(4d-)^1$	1/2	3/2	47.637	47.9029(24)	1.00	1.00
$(4p-)^1$	$(4s+)^1(4p-)^1(4p+)^1$	1/2	1/2	59.876	60.6157(42)	0.67	0.35
$(4p-)^1$	$(4s+)^1(4p-)^1(4p+)^1$	1/2	3/2	60.820	61.3341(21)	0.75	0.62

Table 8. List of predicted and measured transitions in the Zn-like ion W^{44+} (ground state: $(3d)^{10}(4s)^2$ $J = 0$). Wavelength predictions quoted are those by Fournier [6].

Level				Wavelength		Intensity	
Lower	Upper	J_l	J_u	Predicted	Measured	Pred.	Meas.
$(4s+)^1(4p-)^1$	$(4s+)^1(4d+)^1$	1	2	44.384	44.5299(62)	0.01	0.04
$(4s+)^1(4p-)^1$	$(4s+)^1(4d-)^1$	1	2	48.412	48.6165(27)	0.33	0.09
$(4s)^2$	$(4s+)^1(4p+)^1$	0	1	60.665	60.9310(17)	1.00	1.00
$(4s+)^1(4p+)^1$	$(4s+)^1(4d+)^1$	2	2	66.462	66.9301(40)	0.05	0.04

Table 9. List of predicted and measured transitions in the Cu-like ion W^{45+} (ground state: $(3d)^{10}(4s+)^1$ $J = 1/2$). Wavelength predictions quoted are those by Fournier [6].

| Level				Wavelength		Intensity	
Lower	Upper	J_l	J_u	Predicted	Measured	Pred.	Meas.
$(4p-)^1$	$(4d-)^1$	1/2	3/2	49.165	49.2080(63)	0.06	0.26
$(4s+)^1$	$(4p+)^1$	1/2	3/2	62.187	62.3355(19)	1.00	1.00
$(4d-)^1$	$(4f-)^1$	3/2	5/2	68.010	68.1569(28)	0.01	0.04
$(4p+)^1$	$(4d+)^1$	3/2	5/2	71.890	71.9437(503)	0.10	0.08

predicted and measured relative intensities are listed. *The relative intensity* of the calculated transitions means the ratio of the line's collisional-radiative line intensity to that of the strongest predicted line of the same charge state. For a measured line it means the ratio of that line's area to the measured area of the strongest predicted line in that charge state after taking account of the relative intensity calibration. The strongest predicted line is used rather than the strongest measured line so that comparisons to theory can be made.

Figure 2 shows the nine measured charge states of W displayed in a similar fashion to the calculations by Fournier in Fig. 1. Each of the displayed spectra are accumulations of all data taken at each energy after background subtraction. Notice, however, that the apparent baseline for the lower energy charge states is higher than for the higher energies. This suggests the existence of many more unresolved, low-intensity lines adding to a quasi-continuum. This agrees with predictions of many weak N-shell transitions and the measurement of a quasi-continuum found in tokamak and laser plasma spectra at these energies. Even though these EBIT measurements are well resolved in both wavelength and electron energy, a remnant of this feature still persists. A similar quasi-continuum had been noted in the spectra of low-charge states of iron measured on EBIT-II [18].

The most notable difference between the measured and predicted transitions is that the measured lines show a lower than predicted intensity in the 60 Å range as compared to the 45 Å lines. This is exemplified in Fig. 3, where the spectrum obtained at 2.05 keV (optimized for Se-like ions) is shown along with a simulated tungsten spectrum, using Fournier's predictions with weighted contributions (10% As-, 35% Se-, 35% Br-, 15% Kr-, and 5% Rb-like ions). All of the strong features in the measured spectrum appear in the simulated data, albeit, regularly at wavelengths that are about 0.8 Å shorter than predicted. Even after making an adjustment for the energy response of the CCD detector, the shorter wavelength transitions, that is, mostly 4p–4d transitions, appear much stronger than predicted, in relation to the 60 Å band of lines.

The Rb-like ion spectrum is the most complex of the series of ions in this study. With thirty-five bound electrons, the ground state has nine electrons outside of the closed $n = 3$ shell, resulting in a rather complex level system. Adding to this complexity are the many possible allowed transitions in the

Fig. 2. Spectra of tungsten at nine energies that optimize the production of the spectra (ion-charge states) indicated. The intensities have been scaled as described in the text. The raised section within the dotted lines and marked by an asterisk (*) is an artifact that is due to the C K absorption edge in the reference spectrum. Each spectrum is marked by the charge state optimized at that particular energy. The electron-beam energies were 1.79, 1.89, 1.95, 2.05, 2.10, 2.37, 2.46, 2.71, and 3.02 keV for the spectra labeled Rb- through Cu-like, respectively. Typically, ions in three or four other charge states were also present at each setting.
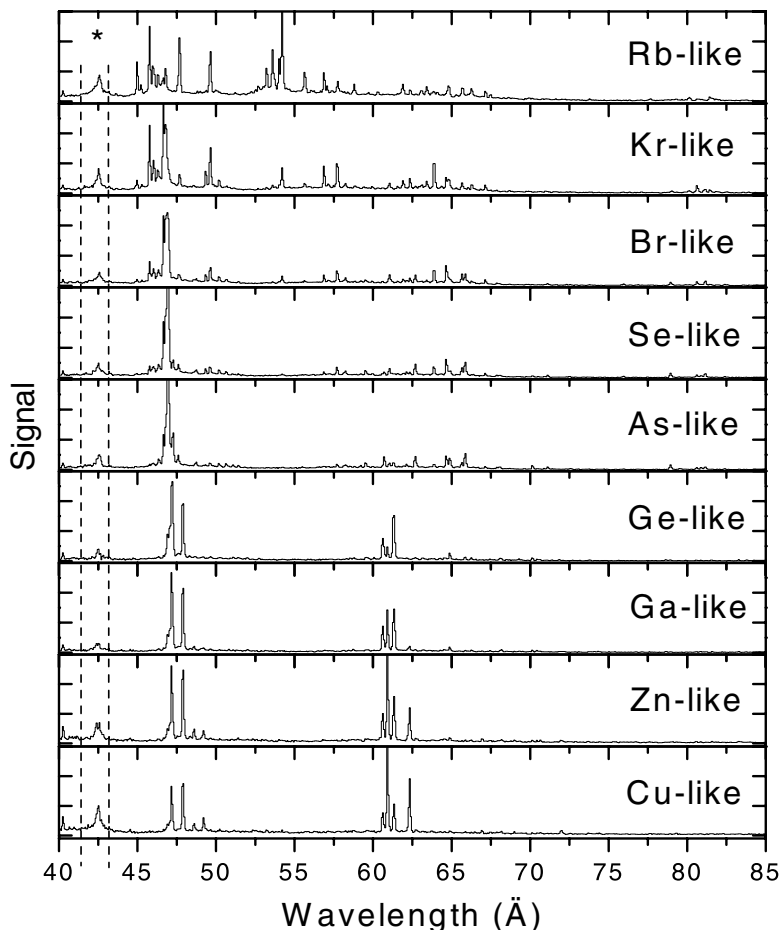
wavelength range 40–80 Å. Ten lines were measured that could be attributed to this charge state. The aforementioned 0.8 Å (roughly 1.5%) wavelength difference between the predicted and observed line positions seems independent of whether the transition is to the ground state or not. Four of the measured lines are believed to be unresolved blends of transition pairs. Each of these states only differs in the total J value of the upper level. The transitions are marked in Tables 1, 3, and 4 by a "b" following the measured wavelength. The second component of each line pair is listed with no measured wavelength. One Rb-like transition ($\lambda_{\text{pred.}} = 60.717$ Å) predicted to be at least as intense as other identified lines was not found.

Removing another electron from the Rb-like ion produces an ion of the Kr sequence. Many fewer lines were predicted for this charge state. Seven were measured, but only three of these could be attributed to predicted Kr-like transitions, even though the other four had intensities that peak at the same beam energy as the other Kr-like lines. Transitions from neighboring states were also checked as candidates, but no satisfactory assignments could be made. The wavelengths of the two most intense measured lines were about 0.6 Å longer than predicted, while the third was at a shorter wavelength. This weak line,

Fig. 3. (*a*) Tungsten spectrum produced under conditions that are optimal for the Se-like ion and (*b*) simulated spectrum based on the calculations by Fournier [6] with several charge states represented at fractions similar to those found in the electron-beam ion-trap spectrum.
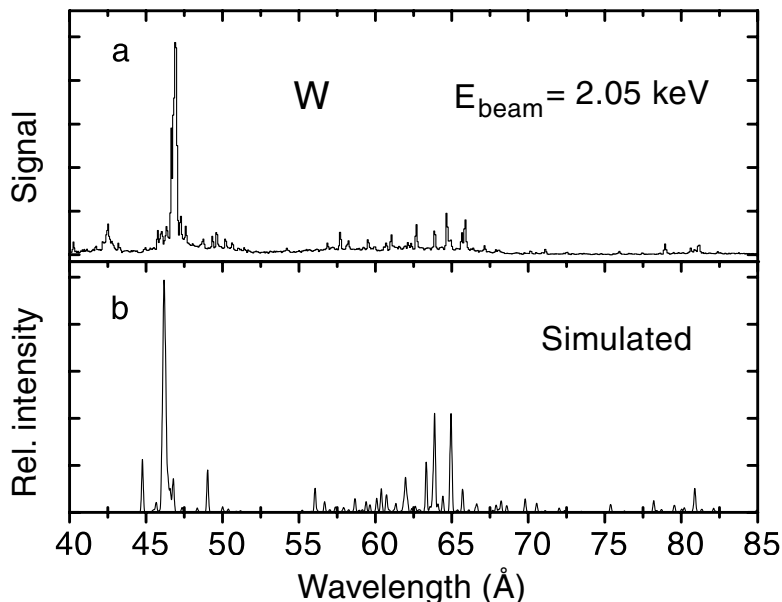
however, had too poor statistics to yield an accurate measurement. The next three higher charge states yielded seven, ten, and seven measured lines, respectively. Most of these lines were found in the line complex at 45 Å. The proximity of lines within this group resulted in an increased uncertainty and scatter of the measured wavelength values. The difference between theory and experiment averaged, again, about 0.6 Å. The final four charge states in this series of ions produced a combined 15 measured lines in this wavelength range. These lines were all well resolved and seen over a wide range of electron-beam energies. Moreover, since the ionization potentials of these charge states are also more widely separated than the others, the wavelength measurements were notably more precise than others. These lines also agreed better with wavelength predictions than those of lower charge states, averaging an offset of only 0.3 Å. The strong line in the Cu-like spectrum showed the smallest (0.1 Å) offset between calculated and measured wavelength value.

5. Discussion

The present measurement of prominent EUV line wavelengths of intermediate-charge-state ions of tungsten shows that fully relativistic ab initio calculations for these spectra can deliver results within about 1% of the correct numbers. In combination with EBIT-II's capability of optimizing the production of individual spectra and of discriminating against others, this level of agreement is sufficient to identify most of the lines in the present tungsten EUV spectra. This, in turn, indicates which corrections need to be applied to theoretical predictions and spectral modeling to be better applicable. Evidently, the particular conditions found in EBIT-II make for spectra that are largely resolvable. Tokamak and laser-produced plasma spectra, in contrast, are so spectrally dense that it rarely is possible to identify individual EUV lines [1–4, 19, 20].

We observed an intensity pattern of lines that originate from the 4p and 4d levels that differs from prediction. It is likely that this reflects level population mechanisms that work differently in our machine than is assumed in the modeling. For example, the calculations referred to here [6] have been tailored for tokamak conditions. Although the typical tokamak ion density is rather similar to that of the ion cloud in

an electron-beam ion trap (typically about one or two orders of magnitude higher), a tokamak plasma has a broad Maxwellian electron-temperature distribution, so that the electron-energy distribution reaches to values much higher and lower than the average. In contrast, EBIT has a very well-defined electron-beam energy with a spread measured to be only about 50 eV. A recalculation of the spectra for conditions more similar to those found in EBIT [21] resulted in some intensities changing by a significant fraction, but none of the strong lines did, and no systematic trend of the intensities was identified.

We chose not to include the ASDEX Upgrade tokamak [2] or Berlin EBIT [8] wavelength results into our tables to avoid clutter and to emphasize the fact that both studies proceeded in parallel. Radtke et al. [8] already give comparisons to the earlier tokamak data [2], featuring an improvement in wavelength precision that is evident by adding a fourth decimal to all of the reported wavelengths. Our spectral resolution (line width FWHM of about 0.12 Å) is slightly better than that reached in the Berlin work (0.2 Å). This is an advantage as it reduces ambiguities in the analysis of many line groups with narrowly spaced components.

Radtke et al. present line identifications and wavelengths for six ions, W^{36+} (Sr-like) to W^{41+} (As-like), five of which overlap with our data. They report 23 identified lines from these ions, while we report 48 (out of about 60 lines total). The charge-state identifications of the lines that are common to both studies agree. The Berlin study claims typical wavelength uncertainties of about 0.05 Å; most of our wavelengths (except for some weak lines) carry uncertainties of less than 0.01 Å. The differences of the results scatter, however, by slightly more than the the combined error estimates. Both studies find similar systematic deviations from the theoretical predictions referred to (in both cases this is basically the HULLAC Hebrew University Lawrence Livermore Atomic Code [22, 23]).

Acknowledgement

References

1. R. Neu, K.B. Fournier, D. Schlögl, and J. Rice. J. Phys. B: At. Mol. Opt. Phys. **30**, 5057 (1997).
2. K. Asmussen, K.B. Fournier, J.M. Laming, R. Neu, J.F. Seely, R. Dux, W. Engelhardt, and J.C. Fuchs. (ASDEX Upgrade Team.) Nucl. Fusion, **38**, 967 (1998).
3. J.F. Seely, C.M. Brown, and U. Feldman. At. Data Nucl. Data Tables, **43**, 145 (1989).
4. C.M. Brown, J.F. Seely, D.R. Kania, B.A. Hammel, C.A. Back, R.W. Lee, and A. Bar-Shalom. At. Data Nucl. Data Tables, **58**, 203 (1994).
5. M.A. Levine, R.E. Marrs, J.R. Henderson, D.A. Knapp, and M.B. Schneider. Phys. Scr. T, **22**, 157 (1988).
6. K.B. Fournier. At. Data Nucl. Data Tables, **68**, 1 (1998).
7. C. Biedermann, R. Radtke, J.-L. Schwob, P. Mandelbaum, R. Doron, T. Fuchs, and G. Fußmann. Phys. Scr. T, **92**, 85 (2001).
8. R. Radtke, C. Biedermann, J.-L. Schwob, P. Mandelbaum, and R. Doron. Phys. Rev. A: At. Mol. Opt. Phys. **64**, 012720 (2001).
9. S.B. Utter, P. Beiersdorfer, and G.V. Brown. Phys. Rev. A: At. Mol. Opt. Phys. **61**, 030503 (2000).
10. E. Träbert, P. Beiersdorfer, K.B. Fournier, S.B. Utter, and K.L. Wong. Can. J. Phys. **79**, 153 (2001).
11. S.B. Utter, G.V. Brown, P. Beiersdorfer, E.J. Clothiaux, and N.K. Podder. Rev. Sci. Instrum. **70**, 284 (1999).
12. T. Harada and T. Kita. Appl. Opt. **19**, 3987 (1980).
13. S.B. Utter, P. Beiersdorfer, J.R. Crespo López-Urrutia, and K. Widmann. Nucl. Instrum. Methods A, **428**, 276 (1999).
14. K. Widmann. Ph.D. thesis. Technische Universität Graz. 1998.

15. H. Chen, P. Beiersdorfer, C.L. Harris, E. Träbert, S.B. Utter, and K.L. Wong. Phys. Scr. T, **92**, 284 (2001).
16. A. Saemann and K. Eidmann. Rev. Sci. Instrum. **69**, 1949 (1998).
17. H. Chen, P. Beiersdorfer, K.B. Fournier, and E. Träbert. Phys. Rev. E: **65**, 056401 (2002).
18. P. Beiersdorfer, J.K. Lepson, G.V. Brown, S.B. Utter, S.M. Kahn, D.A. Liedahl, and C.M. Mauche. Astrophys. J. Lett. **519**, L185 (1999).
19. J. Sugar and V. Kaufman. Phys. Rev. A: Gen. Phys. **21**, 2096 (1980).
20. P. Mandelbaum, M. Finkenthal, J.L. Schwob, and M. Klapisch. Phys. Rev. A: Gen. Phys. **35**, 5051 (1987).
21. K.B. Fournier. Private communication.
22. A. Bar-Shalom, M. Klapisch, and J. Oreg. J. Quant. Spect. Rad. Trans. **71**, 169 (2001).
23. A. Bar-Shalom, M. Klapisch, and J. Oreg. Phys. Rev. A: Gen. Phys. **38**, 1773 (1988).